frontiers | Frontiers in Quantum Science and Technology

TYPE Original Research
PUBLISHED 25 October 2022
DOI 10.3389/frqst.2022.1026025

OPEN ACCESS

EDITED BY
Erik Torrontegui,
Universidad Carlos III de Madrid, Spain

REVIEWED BY
Francesco Plastina,
University of Calabria, Italy
Ricardo Puebla,
Universidad Carlos III de Madrid, Spain

*CORRESPONDENCE
Fernando J. Gómez-Ruiz,
fernandojavier.gomez@iff.csic.es

SPECIALTY SECTION
This article was submitted to Quantum Engineering,
a section of the journal
Frontiers in Quantum Science and Technology

RECEIVED 23 August 2022
ACCEPTED 07 October 2022
PUBLISHED 25 October 2022

CITATION
Higuera-Quintero S, Rodríguez FJ, Quiroga L and Gómez-Ruiz FJ (2022), Experimental validation of the Kibble-Zurek mechanism on a digital quantum computer.
Front. Quantum Sci. Technol. 1:1026025.
doi: 10.3389/frqst.2022.1026025

Experimental validation of the Kibble-Zurek mechanism on a digital quantum computer

Santiago Higuera-Quintero[1], Ferney J. Rodríguez[1], Luis Quiroga[1] and Fernando J. Gómez-Ruiz[2]*

[1]Departamento de Física, Universidad de los Andes, Bogotá, Colombia, [2]Instituto de Física Fundamental IFF-CSIC, Madrid, Spain

The Kibble-Zurek mechanism (KZM) captures the essential physics of nonequilibrium quantum phase transitions with symmetry breaking. KZM predicts a universal scaling power law for the defect density which is fully determined by the system's critical exponents at equilibrium and the quenching rate. We experimentally tested the KZM for the simplest quantum case, a single qubit under the Landau-Zener evolution, on an open access IBM quantum computer (IBM-Q). We find that for this simple one-qubit model, experimental data validates the central KZM assumption of the adiabatic-impulse approximation for a well isolated qubit. Furthermore, we report on extensive IBM-Q experiments on individual qubits embedded in different circuit environments and topologies, separately elucidating the role of crosstalk between qubits and the increasing decoherence effects associated with the quantum circuit depth on the KZM predictions. Our results strongly suggest that increasing circuit depth acts as a decoherence source, producing a rapid deviation of experimental data from theoretical unitary predictions.

KEYWORDS

IBM quantum computing, Kibble-Zurek mechanism, Landau-Zener model, adiabatic-impulse approximation, quantum technologies

Characterizing the non-equilibrium dynamics in noisy intermediate-scale quantum (NISQ) devices plays an important role in developing both hardware and architecture designs in the search for scalable quantum computers. NISQ devices have recently attracted tremendous interest, resulting in rapid progress in fundamental studies of novel hardware and architecture together with promising potential for quantum computing (Preskill, 2018; Bharti et al., 2022). For example, advancements in NISQ devices demonstrate a "quantum advantage" in solving sampling problems (Arute et al., 2019; Zhong et al., 2020; Mooney et al., 2021). To further improve quantum advantage, it is desirable that devices show important features such as high-fidelity gates, qubits with long coherence times, control of state preparation and measurement. (Flammia and Liu, 2011; da Silva et al., 2011; Proctor et al., 2019). Open-access/online NISQ devices have recently become readily available, such as those provided publicly by the IBM Quantum Experience platform (IBM-Corporation, 2022), showing a significant improvement in the last few years. Despite suffering from noise and scalability limitations, this platform

offers a unique possibility to experiment with actual few qubit quantum devices in order to carry out a rigorous study of dynamical quantum properties in different settings along the real time-dynamics of quantum hardware. A key feature of merit in the current NISQ regime is the ability to simulate non-equilibrium quantum dynamics. The Kibble-Zurek mechanism (KZM) (Kibble, 1976; Kibble, 1980; Zurek, 1985; Zurek, 1993) is a prominent paradigm to unravel signatures of universal dynamics in the scenario of a finite-rate spontaneous symmetry breaking. The KZM predicts the production of topological defects (kinks, vortices, strings) or in general, non-equilibrium excitations (in both short- and large-ranged interacting systems) in the course of either quantum (Dziarmaga, 2005; Zurek et al., 2005; Acevedo et al., 2014) or classical (Kibble, 1980; Zurek, 1985) phase transitions. The key result of KZM is concerned with the fact that the mean value of density of topological defects scales as a power law of the quench rate. Furthermore, new evidence of scaling in the high-order cumulants has also been recently shown (Del Campo, 2018; Gómez-Ruiz et al., 2020). These theoretical predictions have been observed in various experimental platforms such as Bose Gas (Goo et al., 2021), trapped ions (Cui et al., 2020), quantum annealer (Bando et al., 2020; King et al., 2022), Bose-Einstein Condensate (Damski and Zurek, 2007; Anquez et al., 2016) and Rydberg atoms (Keesling et al., 2019).

Damski et al. (Damski, 2005; Damski and Zurek, 2006; Cucchietti et al., 2007) established a close relationship between second order quantum phase transitions and avoided level crossing evolutions, thus establishing the Landau-Zener (LZ) model itself as the simplest paradigmatic scenario for probing KZM (Landau, 1932a; Landau, 1932b; Majorana, 1932; Stückelberg, 1932; Zener and Fowler, 1932). The density of topological defects can be expressed as a transition probability for a two-level system. Therefore, this relationship can be tested in generic single qubit platforms. This relationship has been probed by using optical interferometry (Xu et al., 2014), superconducting qubits (Wang et al., 2014; Gong et al., 2016) and trapped ion systems (Cui et al., 2016).

IBM-Q currently grants access up to 5-qubit quantum machines based on superconducting transmon qubits which are controllable using *Qiskit*, an open-source software development kit (Aleksandrowicz et al., 2019; Andersson et al., 2020). These machines have been successfully utilized in simulating spin models (Cervera-Lierta, 2018; Rodriguez-Vega et al., 2022), topological fermionic models (Koh et al., 2022), quantum entanglement (Choo et al., 2018; Wang et al., 2018; Cruz et al., 2019; Mooney et al., 2019; Pozzobom and Maziero, 2019), far-from-equilibrium dynamics (Zhukov et al., 2018), non-equilibrium quantum thermodynamics (Gherardini et al., 2021; Solfanelli et al., 2021), open-quantum systems (García-Pérez et al., 2020), among others. One of the future advantages of IBM-Q is the possibility to do simulation of quantum systems beyond the maximum limits of classical computer over a wide range of parameters. In this work, we test the KZM adiabatic-impulse assumption on the simplest, but important case of a single qubit (LZ model), through experiments on the Qiskit (Andersson et al., 2020) simulator and real quantum hardware, establishing the limits required to obtain accurate results in each case. We successfully reproduced the LZ dynamics under a discrete time evolution in current IBM quantum devices which can provide information about dynamics state evolution given that error mitigation procedures were implemented. Additionally, noticeable effects of decoherence are observed and explained by a simple phenomenological model of relaxation and dephasing for open quantum systems. Furthermore, analysis and estimation of the experimental asymptotic probability allows us to verify the universal KZM in a timescale appropriate for an almost closed system under an adiabatic quench regime. In summary, the key achievement of this work has been the validation of a central premise of KZM through a protocol to characterize and obtain an effective time-dependent dynamics on IBM realistic quantum computers. For reaching such goal we performed LZ evolution under different annealing times, maintaining a fixed number of total gates, a basic benchmark procedure on quantum critical phenomena in near term quantum computers.

This paper is organized as follows. A brief review on KZM, the LZ model and its close connection with KZM are presented in Sect. 1. In Sect. 2 we present the experimental platform. The contrast between theoretical predictions and experimental results is collected in Sect. 3. Finally, we summarize the main conclusions in Sect. 4.

1 Theoretical background

1.1 Brief review of the Kibble-Zurek Mechanism

The KZM describes the dynamics of a system across a continuous symmetry breaking second-order phase transition induced by the change of a control parameter λ. When the system is driven through the critical point λ_c, both the correlation length ξ and reaction time τ diverge as

$$\xi = \xi_0|\epsilon|^{-\nu}, \quad \tau = \tau_0|\epsilon|^{-z\nu}. \tag{1}$$

where, $\epsilon = (\lambda - \lambda_c)/\lambda$ marks the separation from the critical point. The spatial and dynamic *equilibrium* critical exponents are given by ν and z, respectively, while the mesoscopic behavior of the system is contained in the dimensional constants ξ_0 and τ_0. If the quench varies linearly in time, $\epsilon(t) = t/t_a$, where t_a denotes a quench or annealing time scale, the system reaches the critical point at $t = 0$. Therefore, the equilibrium effective reaction time diverges as Eq. 1. This phenomenon is known as critical slowing down and can be used to describe the time evolution across a phase transition as a sequence of three stages. Initially, the system is prepared in the high symmetry

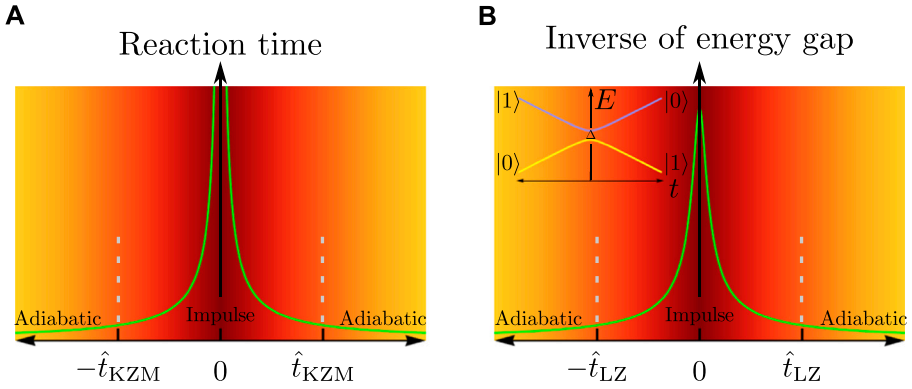

FIGURE 1
Connection between KZM and avoided level crossing in a LZ transition. **(A)** In a continuous second order phase transition, the reaction time diverges near the critical point. The KZM approximation takes into account the total dynamics divided in three stages (adiabatic, impulse and adiabatic) represented by the graduated yellow-dark red-yellow colors and separated by the freeze out-time $\hat{t}_{\mathrm{KZM}}$. **(B)** The inverse of the energy gap in LZ exhibits a similar behavior of the reaction time. However, it is not divergent at the crossing point. Similarly, we divided the LZ dynamics in the same three KZM regimes and separated by the Landau-Zener jump time $\hat{t}_{\mathrm{LZ}}$. Inset: Avoided level crossing LZ.

phase from which it evolves within an adiabatic evolution stage. Secondly, the evolution enters an impulse stage in the neighborhood of the phase transition where the system is effectively frozen. Finally, when the system is far away from the critical point, the dynamics are adiabatic again. These three regimes are schematically represented in Figure 1A. The three regions are separated by two points marked as $-\hat{t}_{\mathrm{KZM}}$ and $\hat{t}_{\mathrm{KZM}}$, in such a way that the freeze-out occurs at the instant $\hat{t}_{\mathrm{KZM}} \sim (\tau_0 t_a^{z\nu})^{1/1+z\nu}$. The main point of the KZM argument is that the size average or correlation length, $\hat{\xi}$, of domains in the broken symmetry phase is set by the equilibrium correlation length evaluated at the freeze-out time. Therefore, the density of excitations resulting from quench evolution scales as $\rho \sim \hat{\xi}^{-D}$ and goes as

$$\rho_{\mathrm{KZM}} \sim \frac{1}{\xi_0}\left(\frac{\tau_0}{t_a}\right)^{\frac{D\nu}{1+z\nu}}, \tag{2}$$

where D is the dimensionality of the system. This result was initially derived in the classical domain (Kibble, 1980; Zurek, 1985) and subsequently extended to quantum systems (Dziarmaga, 2005; Zurek et al., 2005). Additionally, the KZM has also been extended to novel scenarios including long-range interactions (Acevedo et al., 2014; Puebla et al., 2019; Puebla et al., 2020), inhomogeneous systems (Collura and Karevski, 2010; Dziarmaga and Rams, 2010; Gómez-Ruiz and del Campo, 2019) and nonlinear quenches (Barankov and Polkovnikov, 2008; Sen et al., 2008).

1.2 Landau-Zener model

Consider a two-level system, with gap Δ, described by the time-dependent Hamiltonian ($\hbar = 1$)

$$\hat{H}(t) = -\frac{\varepsilon(t)}{2}\hat{\sigma}_z - \frac{\Delta}{2}\hat{\sigma}_x. \tag{3}$$

With $\hat{\sigma}_n$ the Pauli matrix along the $n \in \{x, y, z\}$ direction. We define the *diabatic* states as the Hamiltonian eigenvectors when $\Delta = 0$ and consequently eigenvectors for the Pauli operator $\hat{\sigma}_z$: $\hat{\sigma}_z|0\rangle = +1|0\rangle$ and $\hat{\sigma}_z|1\rangle = -1|1\rangle$. The respective (diabatic) energy levels are $E_{0,1} = \mp\varepsilon(t)/2$. Now, the adiabatic instantaneous eigenvalues $E_\pm(t)$ and eigenstates $|E_\pm(t)\rangle$ are solutions of $\hat{H}(t)|E_\pm(t)\rangle = E_\pm(t)|E_\pm(t)\rangle$. The instantaneous gap energy is given by $\Delta E = E_+ - E_- = \sqrt{\varepsilon^2(t) + \Delta^2}$ (for more details see Ref. (Ivakhnenko et al., 2022)). In the main panel of Figure 1B, we depicted the inverse of the energy gap as a function of time while the instantaneous adiabatic eigenvalues are shown as an inset in the Figure 1B. The eigenstates are written as a linear combination of the diabatic states as $|\psi(t)\rangle = \alpha(t)|0\rangle + \beta(t)|1\rangle$. By solving the corresponding eigenequation in terms of parabolic cylinder functions $\mathbf{D}_p(z)$, and using the substitution $z = t\exp[i\pi/4]/\sqrt{t_a}$, we obtain the transition amplitudes

$$\begin{aligned}\alpha(z) &= \frac{e^{-i\frac{3\pi}{4}}}{\sqrt{\delta}}\left[\delta\chi_1\mathbf{D}_{-1-i\delta}(z) + \chi_2\mathbf{D}_{i\delta}(iz)\right],\\ \beta(z) &= \chi_1\mathbf{D}_{-i\delta}(z) + \chi_2\mathbf{D}_{-1+i\delta}(iz).\end{aligned} \tag{4}$$

where $\delta = \Delta^2 t_a/4$ is the adiabaticity parameter. Moreover, χ_1 and χ_2 are found from the initial condition at $z = z_i$ (see the section: Supplementary Data for details of the calculations and derivations):

$$\begin{aligned}\chi_1 &= \frac{e^{i\frac{3\pi}{4}}\sqrt{\delta}\mathbf{D}_{-1+i\delta}(iz_i)\alpha(z_i) - \mathbf{D}_{i\delta}(iz_i)\beta(z_i)}{\delta\mathbf{D}_{-1-i\delta}(z_i)\mathbf{D}_{-1+i\delta}(iz_i) - \mathbf{D}_{-i\delta}(z_i)\mathbf{D}_{i\delta}(iz_i)},\\ \chi_2 &= \frac{-e^{i\frac{3\pi}{4}}\sqrt{\delta}\mathbf{D}_{-i\delta}(z_i)\alpha(z_i) + \delta\mathbf{D}_{-1-i\delta}(z_i)\beta(z_i)}{\delta\mathbf{D}_{-1-i\delta}(z_i)\mathbf{D}_{-1+i\delta}(iz_i) - \mathbf{D}_{-i\delta}(z_i)\mathbf{D}_{i\delta}(iz_i)}.\end{aligned} \tag{5}$$

Notice that, Eqs 4, 5 are valid for any arbitrary initial condition and final time t. For the experimental implementation discussed below, we are interested in studying the system's evolution from an initial state starting in the anticrossing point at $t = 0$. In the

section: Supplementary Data, the formal solutions for this particular initial condition are summarized.

1.3 Connection between the KZM and LZ evolution

Here we demonstrate how we can implement a controllable evolution using an IBM-Q quantum simulation, in close analogy to the topological defect formation in KZM. Following the seminal arguments exposed in Ref. (Damski, 2005; Damski and Zurek, 2006), topological defects can be built into the LZ model by being associated to the diabatic states. Consider one of the states, such as $|0\rangle$, to be a topologically defected phase and $|1\rangle$ a defect-free phase. For example, in the case of vortices, state $|0\rangle$ may be an eigenstate of the angular momentum operator $\hat{L}_z|0\rangle = n|0\rangle$, while $\hat{L}_z|1\rangle = 0$. In this scenario, Damski introduces the normalized density of topological defects as the average angular momentum

$$\rho_{\mathrm{KZM}} = \frac{1}{n}\langle\psi|\hat{L}_z|\psi\rangle = \left|\langle\psi|0\rangle\right|^2. \tag{6}$$

Then, a system evolving in time under the LZ model can be used to study transitions between the phases through the probabilities of the diabatic states. The similarity between the reaction time of a second order phase transition and the inverse of energy gap in the LZ Hamiltonian is shown in Figure 1B. In analogy with the KZM, this suggests that the adiabatic-impulse-adiabatic approximation (AI) may be used to estimate the asymptotic probability when the system traverses the avoided level crossing, thus elucidating the link between the KZM and LZ evolution.

We divided the dynamics through the anti-crossing into three stages like the AI scenario for KZM. Without loss of generality, we assume that the system starts at $t_i \to -\infty$ from the ground state $|E_-\rangle$, and then it evolves to $t_f \to \infty$. We define a natural time scale given by the inverse of the energy gap

$$\frac{1}{E_+(\hat{t}_{\mathrm{LZ}}) - E_-(\hat{t}_{\mathrm{LZ}})} = \eta\hat{t}_{\mathrm{LZ}}, \tag{7}$$

where $E_\pm(t)$ are the adiabatic energy eigenvalues at time $t = \hat{t}_{\mathrm{LZ}}$ and η is a constant. Using Eq. 3, we obtain

$$\frac{\hat{t}_{\mathrm{LZ}}}{t_a} = \frac{\Delta}{\sqrt{2}}\sqrt{\sqrt{1 + \frac{4}{\left(\Delta^2\eta t_a\right)^2}} - 1}. \tag{8}$$

The AI assumes that the evolution wave function $|\psi(t)\rangle$ of the system satisfies:

- Adiabatic dynamics: from $t_i = -\infty$ to $t = -\hat{t}_{\mathrm{LZ}}$

$$\left|\psi(t)\right\rangle \approx e^{i\Phi_1}\left|E_-(t)\right\rangle.$$

- Impulse dynamics: from $t = -\hat{t}_{\mathrm{LZ}}$ to $t = \hat{t}_{\mathrm{LZ}}$

$$\left|\psi(t)\right\rangle \approx e^{i\Phi_2}\left|E_-(-\hat{t}_{\mathrm{LZ}})\right\rangle.$$

- Adiabatic dynamics: from $t = \hat{t}_{\mathrm{LZ}}$ to $t_f = \infty$

$$\left|\langle\psi(t)|E_-(t)\rangle\right|^2 \approx A.$$

Where Φ_1, Φ_2 are global phases, and A is a constant. Following the AI, Damski in Refs (Damski, 2005; Damski and Zurek, 2006). reported the probability of finding the LZ system in the excited state at $t_f \gg t_{\mathrm{LZ}}$, a calculation we briefly summarize for the sake of completeness in view of our main experimental in terest.

From now on, we focus on the LZ dynamics for the evolution starting in the ground state at the anticrossing point. The initial state at $t = 0$ is then expressed as $|E_-(0)\rangle = (|1\rangle - |0\rangle)/\sqrt{2}$, and consequently the transition probability $P_{\mathrm{AI}} = |\langle E_+(\hat{t}_{\mathrm{LZ}})|E_-(0)\rangle|^2$ is given by (Damski, 2005; Damski and Zurek, 2006)

$$\begin{aligned} P_{\mathrm{AI}} &= \frac{1}{2}\left(1 - \frac{1}{\sqrt{1+\hat{\varepsilon}^2}}\right) \\ &= \frac{1}{2} - \frac{1}{2}\sqrt{1 - \frac{2}{\left(\eta t_a\right)^2 + \eta t_a\sqrt{\left(\eta t_a\right)^2 + 4} + 2}}. \end{aligned} \tag{9}$$

Where we have fixed the two-level system gap to $\Delta = 1$. Additionally, $\hat{\varepsilon} = \varepsilon(\hat{t}_{\mathrm{LZ}})$ is the linear bias at time $t = \hat{t}_{\mathrm{LZ}}$. Expanding Eq. 9 into aseries of $\sqrt{t_a}$, we obtained (Damski, 2005; Damski and Zurek, 2006)

$$P_{\mathrm{AI}} = \frac{1}{2} - \frac{\sqrt{\eta}}{2}t_a^{1/2} + \frac{\eta\sqrt{\eta}}{8}t_a^{3/2} + \mathcal{O}\left(t_a^{5/2}\right). \tag{10}$$

which will be relevant for testing the predictions of the universal AI for KZM below.

2 Experimental IBM-Q platform

We implemented our experimental studies in two topologies or processors types. Figure 2A shows the device layout for the IBMQ 5-qubit ibmq_bogota (Falcon r5.11L topology $\mathcal{QC}_1$) and ibmq_lima (Falcon r4T topology $\mathcal{QC}_2$). The topology of the device determines the possible placement of two-qubit gates. The qubits are furthermore prone to decoherence, thereby requiring several runs of the experiment to make up for statistical errors. We measure the LZ, and concomitant KZM relation, for each one of the IBM-Q transmons in $\mathcal{QC}_1$ and $\mathcal{QC}_2$. Each transmon plays the role of a qubit, evolving with its own dynamics, experimentally showing the effects of decoherence on the hardware. Generally, the physical transmon type qubits of the same machine offer a variety of properties that describe the quality of the qubit, such as thermal relaxation time (T_1), dephasing time (T_2), anharmonicity, and error properties detailed in the section: Supplementary Data, allowing us to

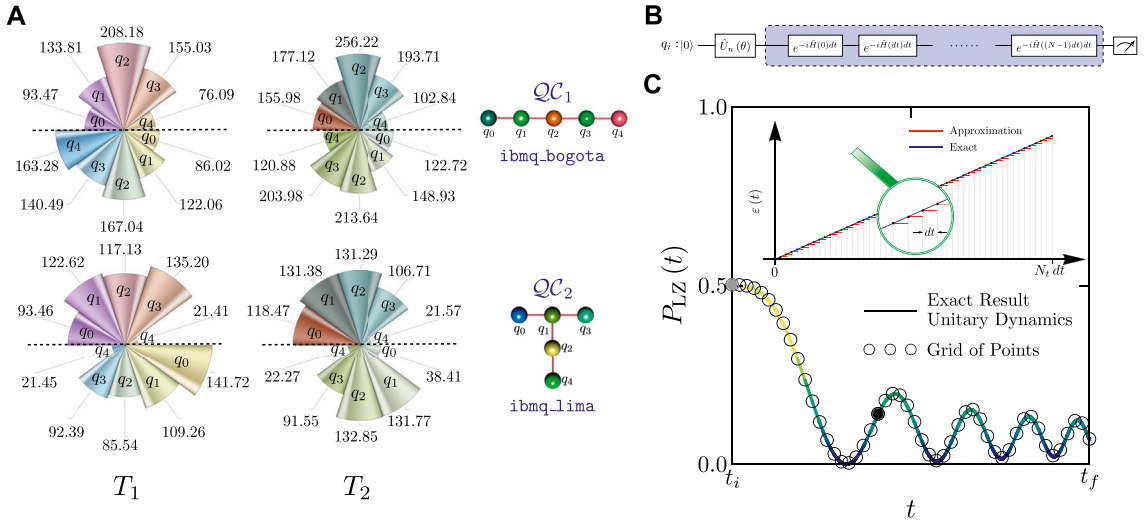

FIGURE 2
Decoherence times in different IBM-Q and IBM-Q circuit simulation of the Landau-Zener process. **(A)** In the pie-like chart, we contrast the thermal relaxation time (T_1) and dephasing time (T_2), in (μs), for two different topology circuits, simply called $\mathcal{QC}_1$ and $\mathcal{QC}_2$ (see text for details). Due to *in situ* IBM machine calibration routines the times T_1 and T_2 may change. Every pie-like chart is divided into two sectors by a dashed line, where the upper and lower sectors corresponding to decoherence times at two different dates. **(B)** Quantum circuit for the LZ simulation starting at the state $|\psi(t_i)\rangle = \hat{U}_n(\theta)|0\rangle$, where $\hat{U}_n(\theta)$ is a unitary rotation along the axis n. **(C)** Schematic representation of the LZ transition probability: the solid line corresponds to the exact result given by Eq. 13, with $\Delta = 1$, $t_a = 2$, $t_i = 0$ and $t_f = 10$, while the symbols illustrate expected results for a grid of points with separation $dt = t_f - t_i/N_t$, being N_t the total circuit depth. The filled dots correspond to: the shortest circuit with depth 1 (gray dot) and an intermediate circuit depth N (black dot). The inset shows the discrete approximation of the time-dependent component $\varepsilon(t)$ of the LZ Hamiltonian.

compare the simulation's performance with different physical parameters. In Figure 2A, the times T_1 and T_2 are depicted for each considered circuit topology at two different dates, illustrating in a graphical way how these times change every time that IBM performed a calibration of every device.

3 Results

3.1 Simulation of the Landau-Zener evolution on IBM-Q

Unitary dynamics.– We are interested in the experimental determination, and respective simulation, on a digital open-access IBM-Q of a single qubit evolution under a linearly time-dependent Hamiltonian (LZ problem). At time t_i, a qubit in the processor is initialized in the state $|\psi(t_i)\rangle = \hat{U}_{\hat{n}}(\theta)|0\rangle$, where $\hat{U}_n(\theta) = \cos[\theta/2]\hat{I} - i\hat{\sigma}_n \sin[\theta/2]$ is a unitary rotation along the axis $n \in \{x, y, z\}$ with $\hat{\sigma}_n$ the usual Pauli matrix along the n-direction. The whole evolution from t_i to t_f is performed by sampling the Hamiltonian at regular intervals $dt = (t_f - t_i)/N_t$ where N_t denotes the number of time steps or the total circuit depth (see blue region in Figure 2B). The equivalent circuit for the experimental IBM-Q realization, and its simulation, is shown in Figure 2B. Assuming an evolution governed by a time-independent Hamiltonian and for small enough intervals of duration dt, the time evolution operator at time $t = N\,dt$, with $1 \leq N \leq N_t$, can be approximated by

$$\hat{U}(t, t_i) \approx \prod_{k=0}^{N-1} e^{-i\hat{H}_k dt}, \tag{11}$$

where $\hat{H}_k = \hat{H}(t_i + kdt)$.

Since we are interested in the evolution from an initial condition where the LZ system is prepared in an equal weight superposition at the anticrossing point, we start by applying the unitary rotation $\hat{U}_y(-\pi/2)$. The approximate time evolution operator is constructed with general unitary gates. A general unitary single qubit gate describes rotations on the Bloch sphere and is defined by three Euler angles

$$\hat{U}(\theta, \phi, \lambda) = \begin{pmatrix} \cos\left(\frac{\theta}{2}\right) & -e^{i\lambda}\sin\left(\frac{\theta}{2}\right) \\ e^{i\phi}\sin\left(\frac{\theta}{2}\right) & e^{i(\phi+\lambda)}\cos\left(\frac{\theta}{2}\right) \end{pmatrix}. \tag{12}$$

IBM-Q devices are equipped with the finite and complete set $\{CX, I, U_z, \sqrt{X}, X\}$ of basis gates on which any quantum circuit must be decomposed into. The general unitary gate can then be expressed using the previous set as $U(\theta, \phi, \lambda) = e^{i\gamma}\hat{U}_z(\phi + \pi)\sqrt{X}\hat{U}_z(\theta + \pi)\sqrt{X}\hat{U}_z(\lambda)$, where $\gamma = (\lambda + \phi + \pi)/2$ is a global phase factor. Using this decomposition, small time progressions as defined in Eq. 11 are simulated and finally the state $|\psi(t)\rangle$ is measured.

As already stated, the Landau-Zener dynamics can be exactly solved (see Supplementary Data), thus allowing a direct benchmark

test of the experimental results on a realistic quantum device against exact results. For a LZ evolution starting at the anticrossing ground state, we obtain the LZ transition probability $P_{\mathrm{LZ}}(t)$ at time t given as

$$P_{\mathrm{LZ}}(t) = |\chi_1 \mathbf{D}_{-i\delta}(z) + \chi_2 \mathbf{D}_{-1+i\delta}(iz)|^2, \tag{13}$$

with the amplitudes χ_1 and χ_2, see Eq. 5, given by:

$$\chi_1 = -\frac{2^k \exp[i\pi k]}{4\sqrt{ik}}\left[\frac{\sqrt{2ik}\,\Gamma(k) + (1+i)\Gamma\left(\frac{1}{2}+k\right)}{\Gamma(2k)}\right], \tag{14}$$

$$\chi_2 = \frac{\exp[i\pi k]}{2^{k+1}}\left[\frac{2ik\Gamma\left(\frac{1}{2}-k\right) + (1-i)\sqrt{2ik}\,\Gamma(1-k)}{\Gamma(1-2k)}\right]. \tag{15}$$

Where z and δ are given in Section 1.2.

Our first aim is to benchmark our LZ experimental results with the above exact theoretical prediction. This is schematically illustrated in Figure 2C where we display the exact result, see Eq. 13, and a hypothetical grid of points representing expected target data with a separation $dt = (t_f - t_i)/N_t$, being N_t the total circuit depth. For every experimental data, 5,000 shots have been realized on each quantum circuit, $\mathcal{QC}_1$ and $\mathcal{QC}_2$.The unit of energy is set by choosing $\Delta = 1$ in the LZ Hamiltonian (see Eq. 3). Therefore, in the following, we express energy parameters and time as dimensionless quantities ($\hbar = 1$). Using the quantum circuits $\mathcal{QC}_1$ and $\mathcal{QC}_2$, we implemented the corresponding gates in all qubits available on parallel and we did a sweep of parameters in annealing time t_a from 0.05 to 2.0. Additionally, for both theoretical and experimental results, the final evolution time t_f was chosen according with: $t_f = 4$ for annealing times in the interval $0.05 \leq t_a \leq 0.17$ and $t_f = 10$ for $0.17 < t_a \leq 2$. These particular choices have been supported by the fact that as we are mainly interested in the asymptotic LZ probability transition, a good asymptotic collapse is reached for these parameter regimes. We also represent the experimental results $P_{\mathrm{LZ}}(N)$ as a function of the number of layers in the circuit instead of time. We emphasize that an N-deep circuit corresponds to a physical qubit interaction time $t_{\mathrm{Int}} = 2t_{SX}N$, where t_{SX} is the gate length property for $\sqrt{X}$ and it is fixed by IBM-Q as $t_{SX} = 35.555$ ns. In Figure 3, we present a contrast of the LZ transition probability for both the theoretical and experimental results. In the panel Figure 3A, we choose the most robust qubit that better reproduced the theoretical P_{LZ}. Specifically, we found that the qubit 3 and 2 for ibmq_bogota and ibmq_lima, respectively, have the best performance. In order to better appreciate the experimental agreement and differences for every single-qubit over $\mathcal{QC}_1$ and $\mathcal{QC}_2$, we show the LZ transition probability as a function of the number of applied gates in Figure 3B.

In the next subsection, we address the influence of the number of layers in the LZ simulation circuit and the role of decoherence.

Open system dynamics.- The performance of the hardware worsens with an increasing depth of the circuit. The assumption of a closed quantum system rapidly breaks down for qubits with short relaxation (T_1) and dephasing (T_2) timescales, thus requiring for a theoretical analysis that resorts to a quantum open system approach. The effects of quantum decoherence are noticeable in the measured probability when scaling the number of gates due to the increase in computing times. We model every qubit on IBM-Q as a two-level system coupled to a Markovian bath. The system evolution is described by a continuous map $\rho_t = e^{t\mathcal{L}}\rho_{t_0}$, $t \geq 0$ generated by the Lindbladian $\mathcal{L}[\bullet] = -i[\hat{H}, \bullet] + \sum_n (\hat{L}_n \bullet \hat{L}_n^\dagger - \frac{1}{2}\{\hat{L}_n^\dagger \hat{L}_n, \bullet\})$ (Breuer and Petruccione, 2007), where, $\hat{H}$ is the Hamiltonian and $\{\hat{L}_n\}$ are Lindblad operators that describe the system-bath interactions. Dissipative processes in a superconducting qubit such as relaxation, i.e., transitions from the higher energy level $|1\rangle$ to ground state $|0\rangle$, can be described phenomenologically by the operator $\hat{L}_1 = \sqrt{\Gamma}|0\rangle\langle 1|$ and dephasing by rotations around the z axis $\hat{L}_2 = \sqrt{\gamma}\hat{\sigma}_z$. Additional transitions such as thermal excitations from the ground state $|0\rangle$ to $|1\rangle$ may also be considered (Marquardt and Püttmann, 2008), although for a superconducting transmon qubit this process is negligible. The rates $\Gamma = 1/T_1$ and $\gamma = 1/T_2 - 1/2T_1$ are related to the characteristic times of each physical qubit.

In Figure 4, we establish a contrast between the unitary exact dynamics, numerical Lindblad dynamics (QuTip) and the experimental results obtained for qubit 4, the noisiest qubit in both quantum machines. QuTiP is an open-source framework for Python that allows for numerical simulations of quantum dynamics of open systems under different solvers (Johansson et al., 2012; Johansson et al., 2013). Specifically, we depicted the Landau-Zener probability as a function of the number of layers in the circuit, N, for two specific annealing times $t_a = 1$ (colors green/purple) and $t_a = 0.1$ (colors blue/orange). Additionally, we show as an inset the ratio between T_2/T_1, the bar scale shows the value of this proportion from 0 to 2. Although, ibmq_lima quantum computer has the ratio T_2/T_1 almost constant, qubit 4 is the most prone to decoherence.

3.2 Simulation of the Kibble-Zurek mechanism on IBM-Q

The main purpose of this work is to validate the adiabatic-impulse approximation of the Kibble-Zurek mechanism through the nonequilibrium dynamics of the Landau-Zener model on IBM-Q. Using Eq. 13 with $\Delta = 1$, the asymptotic probability can be exactly calculated as

$$P_{\mathrm{LZ}}(t \to \infty) = 1 - \frac{1}{\delta}\exp\left[-\frac{3\pi\delta}{2}\right]|\chi_2|^2. \tag{16}$$

Expanding the asymptotic probability into series, we obtain (Damski, 2005; Damski and Zurek, 2006)

$$P_{\mathrm{LZ}}(t \to \infty) = \frac{1}{2} - \frac{\sqrt{\pi}}{4}t_a^{1/2} + \frac{\sqrt{\pi}}{32}(\pi - \ln(4))t_a^{3/2} + \mathcal{O}(t_a^{5/2}). \tag{17}$$

We find the value of η by directly comparing the adiabatic-impulse approximation given by Eq. 10 and the expansion of the LZ asymptotic probability at first-order ($\eta = \pi/4$). However, non-trivial corrections for high-order terms appear. In both main

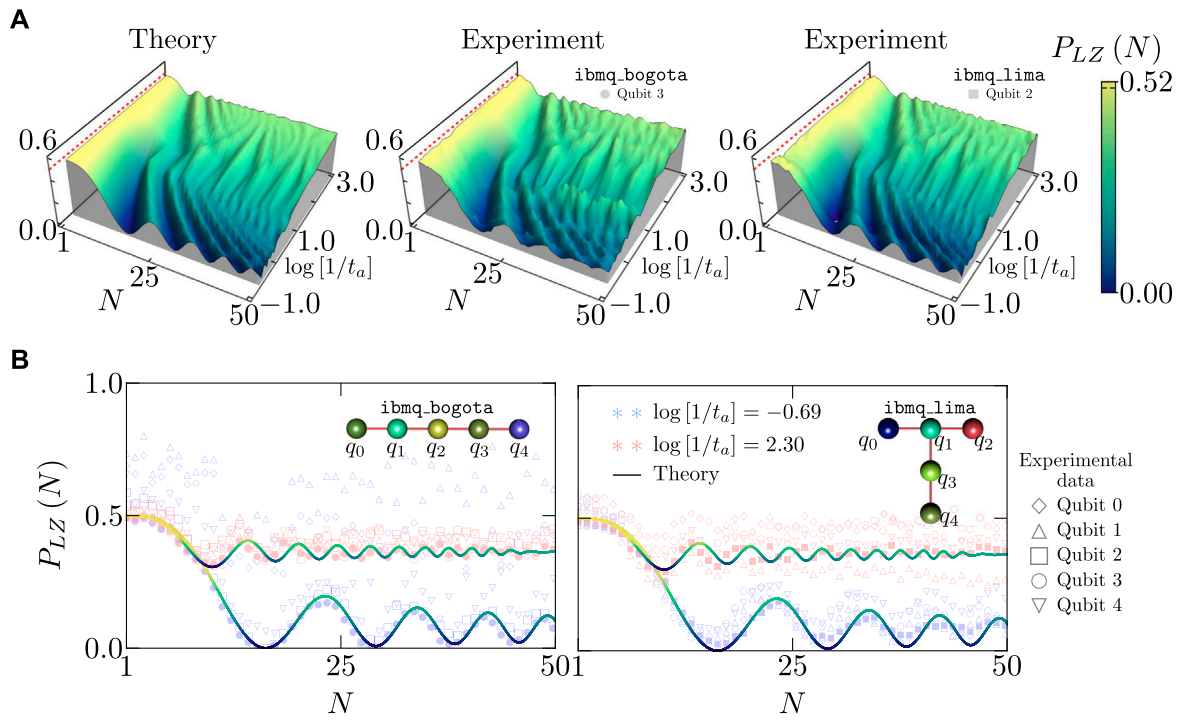

FIGURE 3
Measurement of LZ probabilities on IBM-Q. In panel **(A)**, we establish a contrast between the exact and experimental results for the LZ transition probability as a function the number of layers or circuit depth N, and the annealing time t_a. In this panel, all figures share the same color vertical scale. The initial condition, $P_{LZ}(t = 0) = 0.5$, is represented by a red dashed line. Note that in some region of parameters a probability larger than 0.5 for the experimental results is obtained. In panel **(B)**, the behavior of the LZ probability for every qubit available in each processor is shown, identifying in this way the most isolated (larger decoherence time) qubit in each case. We fixed the maximum number of layers in the circuit as $N_t = 50$.

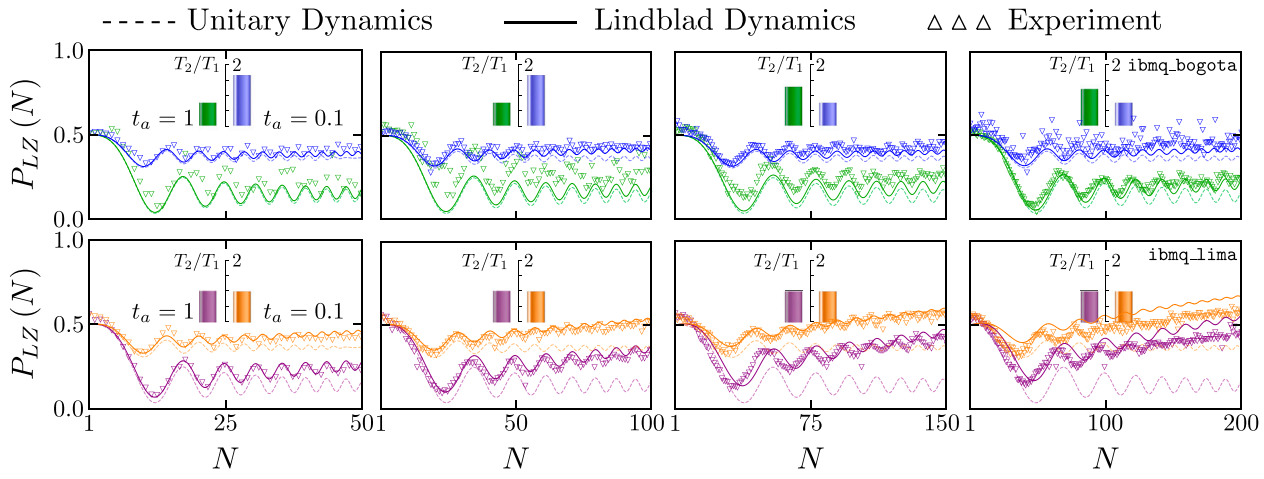

FIGURE 4
Contrast between close and open quantum dynamics for LZ on IBM-Q. The Landau-Zener transition probability is shown as a function of the number of layers N in the circuit implemention for qubit 4, the noisiest qubit for each $\mathcal{QC}_1$ and $\mathcal{QC}_2$ quantum circuit. We contrast the theoretical prediction for a close system (unitary dynamics) given by Eq. 13 (dashed line), the decoherent dynamics given by the numerical solution of the Lindblad equation (solid line) and experimental results (symbols). The experimental results clearly depart from the unitary evolution prediction as the number of layers N_t increases in the circuit (see Figure 2B blue region). Additionally, in every panel, we present as inset the ratio between the dephasing time (T_2) and the thermal relaxation time (T_1).

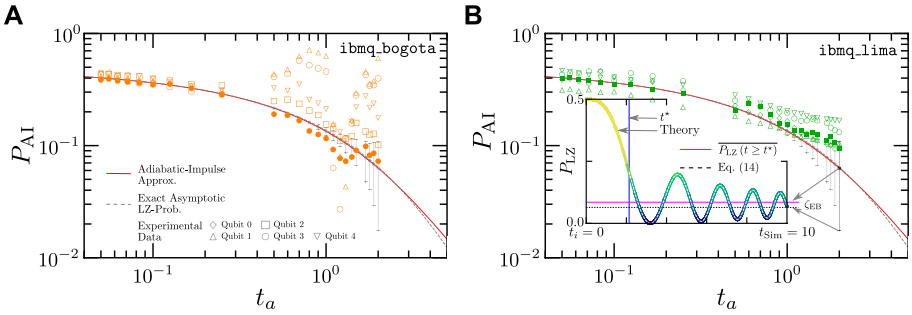

FIGURE 5
Simulation of the Kibble-Zurek mechanism on IBM-Q. In both upper and lower panels, we contrast the adiabatic-impulse approximation (Eq. 9), asymptotic Landau-Zener probability (Eq. 16), and the experimental data. In panel **(A)**, we show experimental data retrieved from ibmq_bogota. In panel **(B)**, we present the experimental results from ibmq_lima. In the inset, we present the protocol to calculate the asymptotic experimental Landau-Zener probability. The error bars with length $2\zeta_{EB}$, calculated from the finite-time effect, are also shown. Solid symbols are consistent with the best qubit behavior as depicted in Figure 3.

panels of Figures 5A,B, we depict the agreement of the theoretical prediction for the adiabatic-impulse approximation (Eq. 9) and asymptotic Landau-Zener probability (Eq. 16). We note the role of the corrections for large quench times. For finite-time LZ simulations, estimating the asymptotic transition probability becomes challenging and similar to experimental data. To this end, we introduced the Landau-Zener jump-time $t^\star$ as the fist zero in the second derivative of the Landau-Zener probability, thus:

$$\left.\frac{d^2 P_{\rm LZ}(t)}{dt^2}\right|_{t=t^\star} = 0. \tag{18}$$

In this way, we propose that the estimated finite-time asymptotic Landau-Zener probability can be approximated by the average of all values of $P_{\rm LZ}(t)$ with $t \geq t^\star$. In the inset of Figure 5B, we display the protocol implemented to calculate the finite-time asymptotic Landau-Zener probability. Therefore, we establish a finite-time error regime depicted in the main panel of Figures 5A,B as error bars using the experimental values of the annealing time. The estimation of the Landau-Zener jump-time $t^\star$ has been implemented uniquely from the theoretical prediction, assuming it will be the same for the experimental data. Note that the adiabatic-impulse approximation and the asymptotic Landau-Zener probability are equivalent in the regime of our experimental data giving confidence in our validation of the KZM on the IBM-Q platform.

For the qubit with the largest decoherence T_1 and T_2 times (the best qubit from now on), the experimental data show an excellent agreement with the theoretical predictions for the impulse-adiabatic approximation. For large annealing time t_a, the experimental data has a significant deviation for some qubits in the ibmq_bogota quantum computer. Indeed, the adiabatic-impulse approximation relationship with the Landau-Zener problem assumes a close system's quantum dynamics. However, since IBM-Q is benchmarked as an open-quantum system, deviations are to be expected.

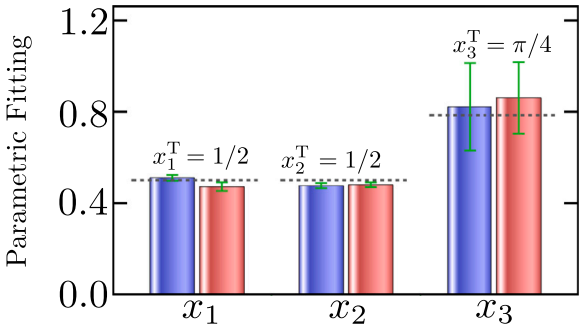

FIGURE 6
KZM adiabatic-impulse approximation fitting parameters. From the best qubit experimental data (solid symbols in Figure 5), the fitting to the KZM adiabatic-impulse approximation $P_{AI}(t_a)$ given by Eq. 19 is probed (the dashed gray lines correspond to the theoretical predictions). The experimental data at ibmq_bogota and ibmq_lima are depicted in blue and red, respectively.

In order to further testing the KZM adiabatic-impulse approximation, from our experimental data, we rewrite the Eq. 9 in terms of 3 fitting parameters, as

$$P_{AI}(t_a) \simeq x_1 - x_2\sqrt{1 - \frac{2}{(x_3 t_a)^2 + x_3 t_a\sqrt{(x_3 t_a)^2 + 4} + 2}}. \tag{19}$$

In Figure 6, we depict the comparison of the fitting parameters x_1, x_2 and x_3 for the best qubit at ibmq_bogota and ibmq_lima. The structure of the fitting expression allows us a direct comparison with the theoretical predictions $(x_1^{\rm T}, x_2^{\rm T}, x_3^{\rm T})$. The first fitting parameter x_1 provides information about how robust the qubit is to decoherence for fast LZ driving. Note that the

theoretical prediction is $x_1^{\mathrm{T}} = 1/2$ as it is fixed by the initial condition at the anticrossing initial point. Moreover, it fixes the value of the impulse-adiabatic approximation for small annealing times, $P_{\mathrm{AI}}(t_a \to 0) = 1/2$. It is evident from Figure 5 that some qubits deviate from this ideal value in this regime, confirming that these qubits are already highly sensible to decoherence. Nonetheless, for these results, we used the smallest number of layers considered. The second fitting parameter x_2 gives information about the higher annealing time regime, with theoretical value $x_2^{\mathrm{T}} = 1/2$. The asymptotic value of the adiabatic-impulse approximation is zero for large annealing times. However, large annealing times imply that the LZ transition probability has several oscillations as a function of time. Consequently, it is necessary to manage large simulation times to obtain the asymptotic LZ probability. It is to be expected that, our results show deviations due to finite simulation time effects. Finally, the third parameter x_3 validates the Kibble-Zurek scaling in the adiabatic-impulse approximation ($x_3^{\mathrm{T}} = \pi/4$). We found an excellent agreement with the theoretical predictions for these $\mathcal{QC}_1$ and $\mathcal{QC}_2$ robust qubits. Thus, by using the close relationship between the KZM and the LZ transition probability, we validated and tested the KZM on IBM-Q. These results can be part of a sequence of major steps to fully understand the strength and limitations of time-dependent quantum simulations. It may provide insights for designing top efficient quantum simulation protocols for more involved out-of-equilibrium and interacting systems.

4 Conclusion

In this work we explored the dynamics of a two level system under the time-dependent Landau-Zener Hamiltonian on digital IBM Quantum computers. Time evolution was simulated by discretization of the time dependent Hamiltonian and application of subsequent single-qubit unitary gates representing finite time progressions. We studied the Landau Zener transition probability as a function of time by running parallel quantum circuits on 5-qubit machines ibmq_lima and ibmq_bogota with different topologies. We find a strong agreement with the theoretical solution of the LZ problem for robust qubits from both machines. We also considered the effect of decoherence on an open LZ system, modeling the dissipation using collapse operators for relaxation and dephasing. For greater trotterizations of the time evolution operator, increasing computing time cause noticeable deviations from the theoretical LZ solution. The numerical solution of the Lindblad master equation accurately depicts the open system's relaxation towards the ground state, supported by the measured probabilities.

The above positive LZ results allowed us to demonstrate the first simulation on a realistic quantum computer of the universal Kibble-Zurek mechanism by estimating the asymptotic transition probability obtained from LZ experimental data. Results show excellent agreement for the best qubits considered in each device and low annealing times. We find that larger annealing times demand a greater time resolution in the evolution operator discretization, putting practical limits on the performance achieved, as it becomes limited by the conflict between computing depth and decoherence times. However, the rapid rate of quantum hardware advances may soon change this. Furthermore, an interesting follow-up research direction would consist in focusing on richer open quantum platforms, where KZM has been poorly explored. Thus, using real quantum hardware to test quantum universal dynamical behaviors, in both closed and open systems, represent an interesting extension of the results presented in this work.

Data availability statement

The datasets presented in this study can be found in online repositories. The names of the repository/repositories and accession number(s) can be found below: https://github.com/sanhq17/Testing_KZM_IBMQ.

Author contributions

FG-R and LQ initiated and guided the project. SH-Q took the experimental measurements. FG-R developed numerical simulations and prepared the figures. All authors contributed to the analysis of the results and the writing of the manuscript.

Funding

SH-Q, FR, and LQ are thankful for the financial support from Facultad de Ciencias-UniAndes projects: INV-2021-128-2292, and INV-2019-84-1841. FG-R acknowledges financial support from European Commission FET-Open project AVaQus GA 899561.

Acknowledgments

The authors thank to Bogdan Damski for useful comments and suggestions.

Conflict of interest

The authors declare that the research was conducted in the absence of any commercial or financial relationships that could be construed as a potential conflict of interest.

Publisher's note

All claims expressed in this article are solely those of the authors and do not necessarily represent those of their

affiliated organizations, or those of the publisher, the editors and the reviewers. Any product that may be evaluated in this article, or claim that may be made by its manufacturer, is not guaranteed or endorsed by the publisher.

Supplementary material

The Supplementary Material for this article can be found online at: https://www.frontiersin.org/articles/10.3389/frqst.2022.1026025/full#supplementary-material

.

References

Abbas, A., Andersson, S., Asfaw, A., Corcoles, A., Bello, L., Ben-Haim, Y., et al. (2020). *Learn quantum computation using Qiskit*.

Acevedo, O. L., Quiroga, L., Rodríguez, F. J., and Johnson, N. F. (2014). New dynamical scaling universality for quantum networks across adiabatic quantum phase transitions. *Phys. Rev. Lett.* 112, 030403. doi:10.1103/PhysRevLett.112.030403

Aleksandrowicz, G., Alexander, T., Barkoutsos, P., Bello, L., Ben-Haim, Y., Bucher, D., et al. (2019). Qiskit: An open-source framework for quantum computing. doi:10.5281/zenodo.2562111

Anquez, M., Robbins, B. A., Bharath, H. M., Boguslawski, M., Hoang, T. M., and Chapman, M. S. (2016). Quantum Kibble-Zurek mechanism in a spin-1 Bose-Einstein condensate. *Phys. Rev. Lett.* 116, 155301. doi:10.1103/PhysRevLett.116.155301

Arute, F., Arya, K., Babbush, R., Bacon, D., Bardin, J. C., Barends, R., et al. (2019). Quantum supremacy using a programmable superconducting processor. *Nature* 574, 505–510. doi:10.1038/s41586-019-1666-5

Bando, Y., Susa, Y., Oshiyama, H., Shibata, N., Ohzeki, M., Gómez-Ruiz, F. J., et al. (2020). Probing the universality of topological defect formation in a quantum annealer: Kibble-Zurek mechanism and beyond. *Phys. Rev. Res.* 2, 033369. doi:10.1103/PhysRevResearch.2.033369

Barankov, R., and Polkovnikov, A. (2008). Optimal nonlinear passage through a quantum critical point. *Phys. Rev. Lett.* 101, 076801. doi:10.1103/PhysRevLett.101.076801

Bharti, K., Cervera-Lierta, A., Kyaw, T. H., Haug, T., Alperin-Lea, S., Anand, A., et al. (2022). Noisy intermediate-scale quantum algorithms. *Rev. Mod. Phys.* 94, 015004. doi:10.1103/RevModPhys.94.015004

Breuer, H. P., and Petruccione, F. (2007). *The theory of open quantum systems*. Oxford, United Kingdom: Oxford University Press. doi:10.1093/acprof:oso/9780199213900.001.0001

Cervera-Lierta, A. (2018). Exact Ising model simulation on a quantum computer. *Quantum* 2, 114. doi:10.22331/q-2018-12-21-114

Choo, K., von Keyserlingk, C. W., Regnault, N., and Neupert, T. (2018). Measurement of the entanglement spectrum of a symmetry-protected topological state using the IBM quantum computer. *Phys. Rev. Lett.* 121, 086808. doi:10.1103/physrevlett.121.086808

Collura, M., and Karevski, D. (2010). Critical quench dynamics in confined systems. *Phys. Rev. Lett.* 104, 200601. doi:10.1103/PhysRevLett.104.200601

Cruz, D., Fournier, R., Gremion, F., Jeannerot, A., Komagata, K., Tosic, T., et al. (2019). Efficient quantum algorithms for GHZ and W states, and implementation on the IBM quantum computer. *Adv. Quantum Technol.* 2, 1900015. doi:10.1002/qute.201900015

Cucchietti, F. M., Damski, B., Dziarmaga, J., and Zurek, W. H. (2007). Dynamics of the bose-hubbard model: Transition from a mott insulator to a superfluid. *Phys. Rev. A* 75, 023603. doi:10.1103/PhysRevA.75.023603

Cui, J. M., Gómez-Ruiz, F. J., Huang, Y. F., Li, C. F., Guo, G. C., and del Campo, A. (2020). Experimentally testing quantum critical dynamics beyond the Kibble–Zurek mechanism. *Commun. Phys.* 3, 44. doi:10.1038/s42005-020-0306-6

Cui, J. M., Huang, Y. F., Wang, Z., Cao, D. Y., Wang, J., Lv, W. M., et al. (2016). Experimental trapped-ion quantum simulation of the Kibble-Zurek dynamics in momentum space. *Sci. Rep.* 6, 33381. doi:10.1038/srep33381

da Silva, M. P., Landon-Cardinal, O., and Poulin, D. (2011). Practical characterization of quantum devices without tomography. *Phys. Rev. Lett.* 107, 210404. doi:10.1103/PhysRevLett.107.210404

Damski, B. (2005). The simplest quantum model supporting the Kibble-Zurek mechanism of topological defect production: Landau-Zener transitions from a new perspective. *Phys. Rev. Lett.* 95, 035701. doi:10.1103/PhysRevLett.95.035701

Damski, B., and Zurek, W. H. (2006). Adiabatic-impulse approximation for avoided level crossings: From phase-transition dynamics to Landau-Zener evolutions and back again. *Phys. Rev. A* 73, 063405. doi:10.1103/PhysRevA.73.063405

Damski, B., and Zurek, W. H. (2007). Dynamics of a quantum phase transition in a ferromagnetic bose-einstein condensate. *Phys. Rev. Lett.* 99, 130402. doi:10.1103/PhysRevLett.99.130402

Del Campo, A. (2018). Universal statistics of topological defects formed in a quantum phase transition. *Phys. Rev. Lett.* 121, 200601. doi:10.1103/PhysRevLett.121.200601

Dziarmaga, J. (2005). Dynamics of a quantum phase transition: Exact solution of the quantum Ising model. *Phys. Rev. Lett.* 95, 245701. doi:10.1103/PhysRevLett.95.245701

Dziarmaga, J., and Rams, M. M. (2010). Dynamics of an inhomogeneous quantum phase transition. *New J. Phys.* 12, 055007. doi:10.1088/1367-2630/12/5/055007

Flammia, S. T., and Liu, Y. K. (2011). Direct fidelity estimation from few pauli measurements. *Phys. Rev. Lett.* 106, 230501. doi:10.1103/PhysRevLett.106.230501

García-Pérez, G., Rossi, M. A. C., and Maniscalco, S. (2020). IBM Q experience as a versatile experimental testbed for simulating open quantum systems. *npj Quantum Inf.* 6, 1. doi:10.1038/s41534-019-0235-y

Gherardini, S., Belenchia, A., Paternostro, M., and Trombettoni, A. (2021). End-point measurement approach to assess quantum coherence in energy fluctuations. *Phys. Rev. A* 104, L050203. doi:10.1103/PhysRevA.104.L050203

Gómez-Ruiz, F. J., and del Campo, A. (2019). Universal dynamics of inhomogeneous quantum phase transitions: Suppressing defect formation. *Phys. Rev. Lett.* 122, 080604. doi:10.1103/PhysRevLett.122.080604

Gómez-Ruiz, F. J., Mayo, J. J., and del Campo, A. (2020). Full counting statistics of topological defects after crossing a phase transition. *Phys. Rev. Lett.* 124, 240602. doi:10.1103/PhysRevLett.124.240602

Gong, M., Wen, X., Sun, G., Zhang, D. W., Lan, D., Zhou, Y., et al. (2016). Simulating the Kibble-Zurek mechanism of the ising model with a superconducting qubit system. *Sci. Rep.* 6, 22667. doi:10.1038/srep22667

Goo, J., Lim, Y., and Shin, Y. (2021). Defect saturation in a rapidly quenched Bose gas. *Phys. Rev. Lett.* 127, 115701. doi:10.1103/PhysRevLett.127.115701

Higuera-Quintero, S., Gómez-Ruiz, F. J., Rodríguez, F., and Quiroga, L. (2022). Repository for "experimental validation of the kibble-zurek mechanism on a digital quantum computer". This repository will be Available at: https://arxiv.org/abs/2208.01050 (Accessed Aug 23, 2022).

IBM-Corporation (2022). Quantum computing IBM. Available at: https://quantum-computing.ibm.com (Accessed 07 27, 2022).

Ivakhnenko, O. V., Shevchenko, S. N., and Nori, F. (2022). Quantum control via landau-zener-stückelberg-majorana transitions. Available at: https://arxiv.org/abs/2203.16348 (Accessed Oct 3, 2022). doi:10.48550/ARXIV.2203.16348

Johansson, J., Nation, P., and Nori, F. (2013). QuTiP 2: A python framework for the dynamics of open quantum systems. *Comput. Phys. Commun.* 184, 1234–1240. doi:10.1016/j.cpc.2012.11.019

Johansson, J., Nation, P., and Nori, F. (2012). QuTiP: An open-source python framework for the dynamics of open quantum systems. *Comput. Phys. Commun.* 183, 1760–1772. doi:10.1016/j.cpc.2012.02.021

Keesling, A., Omran, A., Levine, H., Bernien, H., Pichler, H., Choi, S., et al. (2019). Quantum Kibble-Zurek mechanism and critical dynamics on a programmable Rydberg simulator. *Nature* 568, 207–211. doi:10.1038/s41586-019-1070-1

Kibble, T. W. B. (1980). Some implications of a cosmological phase transition. *Phys. Rep.* 67, 183–199. doi:10.1016/0370-1573(80)90091-5

Kibble, T. W. B. (1976). Topology of cosmic domains and strings. *J. Phys. A Math. Gen.* 9, 1387–1398. doi:10.1088/0305-4470/9/8/029

King, A. D., Suzuki, S., Raymond, J., Zucca, A., Lanting, T., Altomare, F., et al. (2022). Coherent quantum annealing in a programmable 2000-qubit ising chain. *Nat. Phys.* doi:10.1038/s41567-022-01741-6

Koh, J. M., Tai, T., Phee, Y. H., Ng, W. E., and Lee, C. H. (2022). Stabilizing multiple topological fermions on a quantum computer. *npj Quantum Inf.* 8, 16. doi:10.1038/s41534-022-00527-1

Landau, L. (1932a). Zur theorie der energieubertragung. *Phyz. Z. Sowjetunion* 1, 88.

Landau, L. (1932b). Zur theorie der energieubertragung II. *Phyz. Z. Sowjetunion* 2, 46.

Majorana, E. (1932). Atomi orientati in campo magnetico variabile. *Nuovo Cim.* 9, 43–50. 1924-1942. doi:10.1007/BF02960953

Marquardt, F., and Püttmann, A. (2008). Introduction to dissipation and decoherence in quantum systems. Available at: https://arxiv.org/abs/0809.4403. (Accessed 25 Sep 2008).

Mooney, G. J., Hill, C. D., and Hollenberg, L. C. L. (2019). Entanglement in a 20-qubit superconducting quantum computer. *Sci. Rep.* 9, 13465. doi:10.1038/s41598-019-49805-7

Mooney, G. J., White, G. A. L., Hill, C. D., and Hollenberg, L. C. L. (2021). Whole-device entanglement in a 65-qubit superconducting quantum computer. *Adv. Quantum Technol.* 4, 2100061. doi:10.1002/qute.202100061

Pozzobom, M. B., and Maziero, J. (2019). Preparing tunable Bell-diagonal states on a quantum computer. *Quantum Inf. process.* 18, 142. doi:10.1007/s11128-019-2264-z

Preskill, J. (2018). Quantum computing in the NISQ era and beyond. *Quantum* 2, 79. doi:10.22331/q-2018-08-06-79

Proctor, T. J., Carignan-Dugas, A., Rudinger, K., Nielsen, E., Blume-Kohout, R., and Young, K. (2019). Direct randomized benchmarking for multiqubit devices. *Phys. Rev. Lett.* 123, 030503. doi:10.1103/PhysRevLett.123.030503

Puebla, R., Marty, O., and Plenio, M. B. (2019). Quantum Kibble-Zurek physics in long-range transverse-field Ising models. *Phys. Rev. A* 100, 032115. doi:10.1103/PhysRevA.100.032115

Puebla, R., Smirne, A., Huelga, S. F., and Plenio, M. B. (2020). Universal anti-Kibble-Zurek scaling in fully connected systems. *Phys. Rev. Lett.* 124, 230602. doi:10.1103/PhysRevLett.124.230602

Rodriguez-Vega, M., Carlander, E., Bahri, A., Lin, Z. X., Sinitsyn, N. A., and Fiete, G. A. (2022). Real-time simulation of light-driven spin chains on quantum computers. *Phys. Rev. Res.* 4, 013196. doi:10.1103/physrevresearch.4.013196

Sen, D., Sengupta, K., and Mondal, S. (2008). Defect production in nonlinear quench across a quantum critical point. *Phys. Rev. Lett.* 101, 016806. doi:10.1103/PhysRevLett.101.016806

Solfanelli, A., Santini, A., and Campisi, M. (2021). Experimental verification of fluctuation relations with a quantum computer. *PRX Quantum* 2, 030353. doi:10.1103/PRXQuantum.2.030353

Stückelberg, E. C. G. (1932). Theory of inelastic collisions between atoms. *Helv. Phys. Acta* 5, 369.

Wang, L., Zhou, C., Tu, T., Jiang, H. W., Guo, G. P., and Guo, G. C. (2014). Quantum simulation of the Kibble-Zurek mechanism using a semiconductor electron charge qubit. *Phys. Rev. A* 89, 022337. doi:10.1103/PhysRevA.89.022337

Wang, Y., Li, Y., qi Yin, Z., and Zeng, B. (2018). 16-qubit IBM universal quantum computer can be fully entangled. *npj Quantum Inf.* 4, 46. doi:10.1038/s41534-018-0095-x

Xu, X. Y., Han, Y. J., Sun, K., Xu, J. S., Tang, J. S., Li, C. F., et al. (2014). Quantum simulation of Landau-Zener model dynamics supporting the Kibble-Zurek mechanism. *Phys. Rev. Lett.* 112, 035701. doi:10.1103/PhysRevLett.112.035701

Zener, C., and Fowler, R. H. (1932). Non-adiabatic crossing of energy levels. *Proc. R. Soc. Lond. Ser. A, Contain. Pap. a Math. Phys. Character* 137, 696–702. doi:10.1098/rspa.1932.0165

Zhong, H. S., Wang, H., Deng, Y. H., Chen, M. C., Peng, L. C., Luo, Y. H., et al. (2020). Quantum computational advantage using photons. *Science* 370, 1460–1463. doi:10.1126/science.abe8770

Zhukov, A. A., Remizov, S. V., Pogosov, W. V., and Lozovik, Y. E. (2018). Algorithmic simulation of far-from-equilibrium dynamics using quantum computer. *Quantum Inf. process.* 17, 223. doi:10.1007/s11128-018-2002-y

Zurek, W. H. (1993). Cosmological experiments in condensed matter systems. *Phys. Rep.* 276, 177–221. doi:10.1016/s0370-1573(96)00009-9

Zurek, W. H. (1985). Cosmological experiments in superfluid helium? *Nature* 317, 505–508. doi:10.1038/317505a0

Zurek, W. H., Dorner, U., and Zoller, P. (2005). Dynamics of a quantum phase transition. *Phys. Rev. Lett.* 95, 105701. doi:10.1103/PhysRevLett.95.105701